Materials Advances

ROYAL SOCIETY OF CHEMISTRY

PAPER

View Article Online
View Journal | View Issue



Cite this: *Mater. Adv.*, 2022, 3, 245

# Leaf-like copper oxide mesocrystals by collagen-assisted biomineralization show attractive biofunctional and electrochemical properties†

Huixia He,[a] Wenyu Wei,[a] Yongling An,[b] Jinkui Feng [b] and Jianxi Xiao *[a]

Received 31st August 2021,
Accepted 2nd October 2021

DOI: 10.1039/d1ma00788b

rsc.li/materials-advances

The development of high-performance biocompatible batteries is pivotal in personalized health-care devices such as pacemakers and neuro-stimulators. We have for the first time developed a one-pot collagen-assisted biomineralization strategy to create hierarchical CuO nanostructures. Recombinant collagen has been demonstrated as an excellent biotemplate to delicately tune the morphologies of copper oxide mesocrystals. The initial formation of $Cu(OH)_2$ nanoneedles gradually turned into leaf-like CuO nanostructures with branched edges and a compact middle during the biomineralization process. The as-prepared leaf-like CuO mesocrystals exhibited an attractive electrochemical performance, and may have great potential as a promising anode material for lithium-ion batteries. Notably, collagen also acts as an excellent functional agent to endow the CuO nanomaterials with high biocompatibility and bioactivity. The environmentally friendly method assisted by collagen provides novel opportunities for the construction of advanced CuO nanomaterials that have a well-controlled morphology, function and electrochemical performance, and which may have promising applications in implantable health-care electronics.



## 1. Introduction

Biomineralization is a ubiquitous process in nature that creates inorganic mesocrystals with delicately controlled morphologies and polymorphs.[1–3] Bones, fish scales and shells are classical products of biomineralization in various living organisms. Biomolecular templates such as proteins have been found to play an essential role in the growth and nucleation of these inorganic crystals.[4,5] The exploration of biomolecular building blocks to synthesize hierarchical mesocrystals has gained increasing attention due to their excellent features such as mild reaction conditions and precise tuning of sizes and shapes.[6,7] Proteins have remarkable advantages, such as being an abundant natural resource and having pronounced structural diversity, and they have been extensively investigated to assist the formation of nanostructured materials.[3,6,8]

Metal oxide nanoparticles have been used widely in a range of applications such as energy storage, catalysis and antimicrobics.[9–12] There are many materials used for lithium-ion battery anodes.[13–16] Copper oxide (CuO) has attracted particular interest due to its prestige as a p-type semiconducting material with a narrow band gap of 1.2 eV. It has displayed promising applications in photocatalytic reactions and photovoltaic cells, and it is a noteworthy potential material for lithium-ion battery anodes.[17–22] In addition, the low cost, environmental friendliness and high chemical stability of copper oxide assures it as a favorite candidate for large-scale fabrication.

Extensive efforts have been devoted to synthesizing well-ordered copper oxide nanomaterials with a variety of morphologies ranging from nanorods and nanowires to dumbbells and honeycombs.[23–31] Organic ligands such as acetic, citric, and tartaric acids have been reported to regulate the crystal growth of copper oxide nanostructures through their coordination with copper ions.[29,32,33] Recently, Chen's group has developed a silk fibroin-assisted biomineralization route to synthesize almond-like copper oxide mesocrystals.[34] However, the potential toxicity of the reported copper oxide nanomaterials may not meet the biocompatibility requirements of the rising demand of implantable electrical devices in health-care applications.

Collagen is a unique protein family that contains distinct $(Gly\text{-}X\text{-}Y)_n$ amino acid sequence patterns and a triple-helix structure.[35] The rigid rod-like shape and self-assembly features have distinguished collagen as an excellent building block, which is the major structural component of connective tissues

[a] *State Key Laboratory of Applied Organic Chemistry, Key Laboratory of Nonferrous Metal Chemistry and Resources Utilization of Gansu Province, College of Chemistry and Chemical Engineering, Lanzhou University, Lanzhou 730000, China. E-mail: xiaojx@lzu.edu.cn*
[b] *School of Chemistry and Chemical Engineering, Shandong University, Jinan 250100, China*

† Electronic supplementary information (ESI) available: Fig. S1–S4. See DOI: 10.1039/d1ma00788b

such as skin, bones and teeth.[36] Collagen has been considered as the key biotemplate for the production of hydroxyapatite with delicate hierarchical nanostructures, which determine the mechanical properties and biological function of bones.[37] Collagen has recently been explored to assist the formation of hematite mesocrystals.[38]

Herein, we have for the first time developed a collagen-templated biomineralization strategy to create hierarchical CuO nanostructures with attractive biofunctional as well as electrochemical properties. Collagen has been shown to finely tune the nanostructures of copper oxide, which exhibit a good electrochemical performance and show great potential as a lithium-ion battery anode. Furthermore, collagen functionalizes CuO nanomaterials with high biocompatibility and bioactivity. These novel CuO nanomaterials with a well-controlled morphology, function and electrochemical performance may open promising opportunities in implantable electronics.

## 2. Experimental section

### Preparation of recombinant collagen

Recombinant collagen was expressed in the *E. coli* BL21 strain following previously reported protocols.[39,40] Briefly, cells were grown in 50 ml of LB medium overnight at 37 °C, and transferred to 1 L of LB media. When the $OD_{600\,nm}$ of the culture reached 0.8, 1 mM isopropyl β-D-thiogalactopyranoside (IPTG) was added to induce protein expression at 25 °C. Cells were harvested, and then re-suspended in the binding buffer (20 mM sodium phosphate buffer, pH 7.4, 500 mM NaCl, 20 mM imidazole). The supernatant fraction was collected after cell disruption. Raw proteins were purified using a Ni–NTA-Sepharose column with the elution buffer (20 mM sodium phosphate buffer, pH 7.4, 500 mM NaCl, 500 mM imidazole), and dialyzed against glycine buffer (50 mM, pH 8.6). Recombinant collagen was produced by trypsin digestion of the purified protein, as previously described. The purity of recombinant collagen was confirmed using SDS-PAGE. The pure collagen was dialyzed, lyophilized and stored at −20 °C for future use.

### Synthesis of copper oxide nanostructures

120 mg of $Cu(CH_3COO)_2{\cdot}H_2O$ and 15 mL of 10 mg $mL^{-1}$ collagen solution were added to 12 mL of water, and the mixture was stirred for 1 hour to obtain a blue transparent solution. 3 mL of 1.6 mol $L^{-1}$ NaOH solution was added to the blue solution, and stirred for 30 min. The mixture was then transferred into a 50 mL Teflon-lined stainless-steel autoclave. The autoclave was heated to 80 °C and maintained for 12 hours. The reaction mixture was estimated to contain 0.5 wt% collagen and 0.02 mol $L^{-1}$ $Cu(CH_3COO)_2{\cdot}H_2O$ ([Cu(II)] = 0.02 mol $L^{-1}$). After the autoclave had cooled to room temperature, the precipitates were collected by centrifugation, washed with distilled water and ethanol in turn three times, and dried in air at room temperature. To investigate the effect of collagen on the morphology of nanoparticles, the concentration of collagen was varied from 0.01 to 0.5 wt% while the [Cu(II)] was set as 0.02 mol $L^{-1}$.

### Characterization of copper oxide nanoparticles

Powder X-ray diffraction (XRD) patterns were measured using a Rigaku D/max-2400 X-ray diffractometer (Japan) with Cu Kα radiation (40 kV, 40 mA) at a scanning rate of 0.02° $s^{-1}$ in the $2\theta$ range from 10 to 80°. X-Ray photoelectron spectroscopy (XPS) experiments were performed using a Kratos Axis Ultra$^{DLD}$ X-ray photoelectron spectrometer (England) with a monochrome X-ray source using Al Kα (1486.6 eV) radiation. The binding energies measured *via* XPS were corrected by referencing the C 1s line to 284.5 eV.

FESEM (field-emission scanning electron microscopy) images were acquired using a Hitachi S-4800 field emission scanning electron microscope (Hitachi Limited, Japan) with an operating voltage of 5.0 kV. The dried samples were sputter-coated with Au for 25 s prior to imaging. TEM (transmission electron microscopy), HRTEM (high-resolution transmission electron microscopy), SAED (selected area electron diffraction), and electron diffraction (EDX) measurements were carried out using a JEM-2100 transmission electron microscope (JEOL, Japan) at 200 kV. FT-IR (Fourier transform infrared) spectra were recorded using a Nicolet NEXUS 670 infrared spectrophotometer. TGA (thermogravimetric analysis) experiments were performed using a TGA/NETZSCH STA449 F3 instrument under a nitrogen atmosphere, with a heating rate of 10 °C $min^{-1}$ from 25 °C to 800 °C.

### Electrochemical properties of CuO nanostructures

Copper oxide nanomaterials prepared with 0.5 wt% collagen and 0.02 mol $L^{-1}$ Cu(II) were used for further characterization of the electrochemical performance. 60 wt% of the active material (copper oxide), 20 wt% super P carbon, and 20 wt% binder polyacrylic acid (PAA) were mixed to form a uniform slurry material. Electrodes for electrochemical testing were fabricated by loading the mixed slurry at a rate of 1.5 mg $cm^{-2}$ using a doctor-blade on a Cu foil current collector. The liquid electrolyte was 1.0 M $LiPF_6$ in acetic acid (EC) and dimethyl carbonate (DMC) in 1 : 1 volume ratio and the separator was a Celgard 2400. A half-coin cell was assembled in a glove box using lithium foil as the other electrode. The galvanostatic discharge/charge cycles were measured using an electrochemical workstation (CHI 660E, Shanghai China) in the voltage range between 0.01 and 3 V (*vs.* $Li^+/Li$) at different current densities at a 0.1 mV $s^{-1}$ scan rate.

### Cytotoxicity of leaf-like CuO

Cell counting kit-8 (CCK-8) was used to evaluate the cytotoxicity of the leaf-like CuO nanomaterials using HFF-1 cells. HFF-1 cells were incubated in DMEM culture medium supplemented with 15% bovine serum solution in a humidified atmosphere of 5% $CO_2$ at 37 °C. 100 μL of the HFF-1 cell suspension was added to a 96-well cell-culture plate at a density of $5 \times 10^3$ cells per well, and incubated for 24 hours to allow attachment. 100 μL of leaf-like CuO materials at four different final concentrations

(0.1, 1, 10, and 100 μg $mL^{-1}$) was then added into the wells. An equal volume of DMEM medium was added to other wells as control groups. After incubation for 24 hours, 10 μL of CCK-8 solution (2-(2-methoxy-4-nitrophenyl)-3-(4-nitrophenyl)-5-(2,4-disulfobenzene)-2*H*-tetrazole monosodium salt) was added to each well. The 96-well plate was incubated for 2 hours (5% $CO_2$ at 37 °C). A Tecan Infinite F200/M200 multifunctional microplate reader (Tecan, Männedorf, Switzerland) was used to measure the optical density at 450 nm. The cell viability was calculated as the mean absorption value of four measurements of each condition divided by the mean absorption value of the control group.

### Cell adhesion assay

Nunclon Delta TC Microwell plates were coated with one thin layer of leaf-like CuO. The plates coated with heat-denatured BSA were used as control groups. The plates were washed with PBS three times. Then 100 μL of HFF-1 cell suspension ($1 \times 10^5$ cells per mL) in serum-free DMEM medium was added, and incubated for 6 hours at 37 °C. Unattached cells were washed off with PBS buffer (10 mM). The adhered cells were measured using a total deoxyribonucleic acid (DNA) quantification assay (Hoechst 33258, Solarbio). The cells were lysed by repeated freezing and thawing in ultrapure water. Hoechst 33258 with a final concentration of 5 μg $mL^{-1}$ was added to the cell lysates, and the mixtures were incubated in the dark for 1 hour. The fluorescence intensity was recorded using a microplate reader (Tecan Infinite M200) at the 360 nm excitation wavelength and 465 nm emission wavelength. The measurements were repeated three times.

### Immunofluorescence staining

Fluorescent confocal dishes (non-treated) were coated with one thin layer of leaf-like CuO. The coverslips were washed 3 times with 10 mM, pH 7.4 PBS buffer. Then the HFF-1 cells were added to the coverslips at a density of 400 cells per $mm^2$, and incubated at 37 °C for 24 hours. The attached cells were fixed in cold 4% paraformaldehyde for 10 min, and permeabilized with 0.1% Triton X-100 for 5 min. 1% BSA in PBS buffer (10 mM, pH 7.2–7.4) was used as a blocking agent for 0.5 hours at room temperature. The cells were incubated with phalloidin-tetramethylrhodamine isothiocyanate for 1 hour at 37 °C for the actin cytoskeleton staining. Then DAPI was added for nuclear staining at 37 °C for 10 minutes. The images were acquired using Leica fluorescence microscope (Leica Microsystems Inc., Wetzlar, Germany).

## 3. Results and discussion

### Synthesis and characterization of copper oxide nanostructures

Pure recombinant collagen was produced following previously reported procedures.[39] Collagen was explored as the biotemplate to synthesize copper oxide nanoparticles. Briefly, the mixture of collagen, copper acetate and sodium hydroxide was prepared and incubated at 80 °C for 12 hours to initiate the crystal transformation and assembly of primary copper oxide mesocrystals. The final product was collected for further characterization.

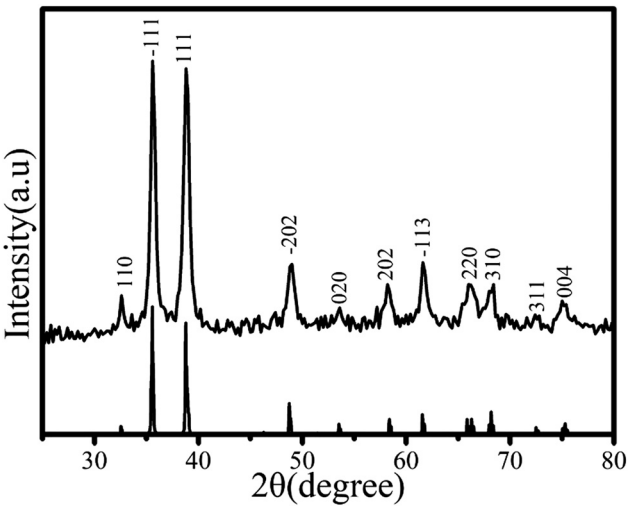


Fig. 1 XRD pattern of the as-prepared copper oxide particles obtained *via* collagen-templated biomineralization ([collagen] = 0.5 wt%, [Cu(II)] = 0.02 mol $L^{-1}$). The standard XRD pattern (copper oxide, JCPDS no. 05-0661) is shown beneath the plot.

X-Ray diffraction (XRD) and X-ray photoelectron spectroscopy (XPS) techniques were employed to investigate the crystal type and elemental composition of the as-prepared products *via* collagen-templated biomineralization (Fig. 1 and Fig. S1, ESI†). The diffraction peaks followed the same pattern as the standard XRD spectrum of pure CuO crystals (copper oxide, JCPDS no. 05-0661) (Fig. 1).[34] The XPS spectra of the as-prepared samples showed characteristic peaks corresponding to Cu $2p_{1/2}$, Cu $2p_{3/2}$ and O 1s, further confirming the presence of CuO (Fig. S1, ESI†). These results indicated that the nanomaterials generated by collagen-templated biomineralization were pure CuO without any other phases such as $Cu_2O$.

Field-emission scanning electron microscopy (FESEM) and transmission electron microscopy (TEM) techniques were applied to characterize the morphology and detailed structure of the synthesized copper oxide mesocrystals (Fig. 2). Copper oxide particles were produced *via* collagen-templated biomineralization with a collagen concentration of 0.5 wt% and a [Cu(II)] of 0.02 mol $L^{-1}$. The SEM images displayed a uniform three-dimensional leaf-like geometry of approximately 1 μm length, 429 nm width and 35 nm thickness (Fig. 2a and b). The magnified SEM image of the leaf-like particles showed that each particle was hierarchical and composed of primary nanoparticle units (Fig. 2b).

The TEM images indicated that the copper oxide mesocrystals were assembled through an oriented growth with primary nanoparticles (Fig. 2c and d). Notably, the leaf-like mesocrystals showed a much more compact middle region than the edges (Fig. 2c and d). The HRTEM image of the middle section showed that most crystalline lattice planes were well aligned, and there were clear gaps between the primary nanoparticles in

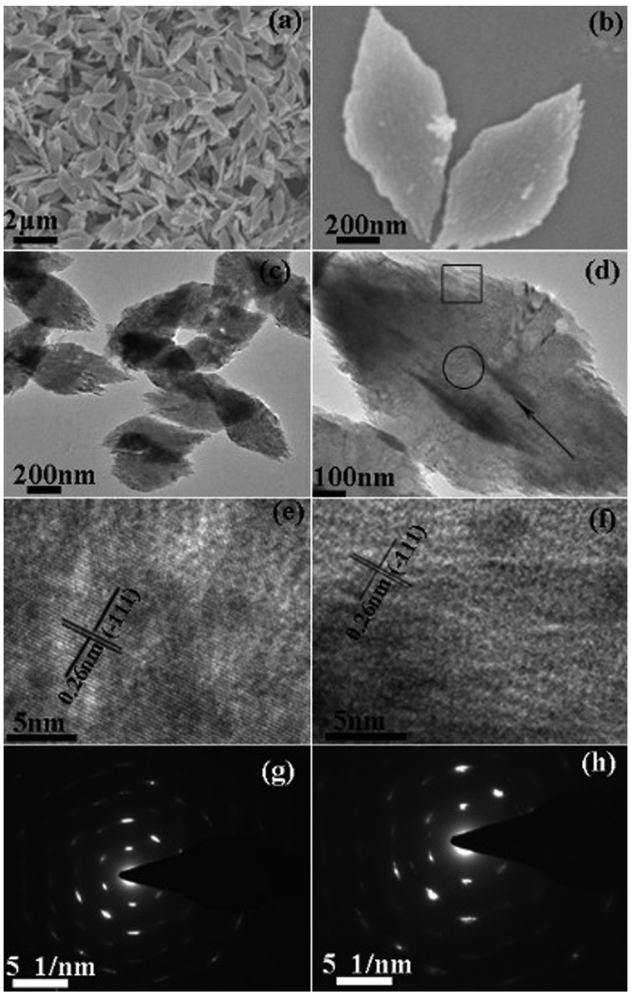


Fig. 2 (a and b) FESEM images of the leaf-like copper oxide mesocrystals obtained after 12 hours *via* collagen-templated biomineralization ([collagen] = 0.5 wt%, [Cu(II)] = 0.02 mol $L^{-1}$); (c and d) TEM images of the same copper oxide particles; (e) HRTEM image of the circle part of (d); and (f) HRTEM image of the square part of (d). (g) SAED pattern of the circle part of (d); and (h) SAED pattern of the square part of (d).

the selected area electron diffraction (SAED) pattern (Fig. 2e). The single-crystal diffraction pattern with relatively short diffraction arcs indicated that the primary copper oxide nanoparticles were arranged in a highly oriented way in the middle region (Fig. 2g). The inter-fringe distance was measured as 0.26 nm, corresponding to the (−111) plane of monoclinic CuO (Fig. 2e). Meanwhile, the HRTEM image of the edges of leaf-like mesocrystals displayed a more random pattern, and elongated diffraction arcs were observed in the corresponding SAED pattern (Fig. 2f and h). These results demonstrated that the lattice planes were stacked in a less orderly fashion at the edges of the leaf-like CuO mesocrystals.

The EDX (energy dispersive X-ray spectroscopy) spectrum of the as-prepared particles indicated the presence of elements C, Cu, and O, demonstrating the inclusion of collagen in the CuO mesocrystals (Fig. S2, ESI†). In addition, the FT-IR spectrum showed vibration peaks corresponding to the N–H, C=C and Cu–O bonds, again confirming the presence of collagen within the CuO particles (Fig. S3, ESI†). All the results indicated that the collagen-templated biomineralization process can generate copper oxide mesocrystals with well-ordered hierarchical structures.

### Time-dependent growth of the leaf-like copper oxide mesocrystals

The FESEM and XRD techniques were simultaneously applied to monitor the time-dependent growth of copper oxide mesocrystals in order to elucidate the self-assembly mechanism of CuO nanostructures using collagen as the biotemplate (Fig. 3). At the initial stage, the mixture of collagen and copper acetate under alkaline conditions led to nanoneedle-like particles after 0.5 hours of incubation (Fig. 3a). The XRD pattern of the as-prepared nanoparticles was assigned to pure $Cu(OH)_2$ (Fig. 4a). This was consistent with a previous report that $Cu^{2+}$ ions readily formed $[Cu(OH)_4]^{2-}$ ions under alkaline conditions, and the decomposition of $[Cu(OH)_4]^{2-}$ tended to result in $Cu(OH)_2$ precipitates with a 1D nanostructure.[41] After 1 hour of reaction, the XRD pattern showed an intermediate stage of the coexistence of $Cu(OH)_2$ and CuO crystalline phases, indicating that a large amount of copper hydroxide particles lost water to form copper oxide (Fig. 4b). The SEM image suggested that primary nanoparticles began to assemble (Fig. 3b). After 3 hours of reaction, the XRD pattern indicated a pure copper oxide crystalline phase (Fig. 4c), and a substantial amount of leaf-like particles had been formed (Fig. 3c). When the reaction was extended to 9 hours, most of the nanoneedles disappeared

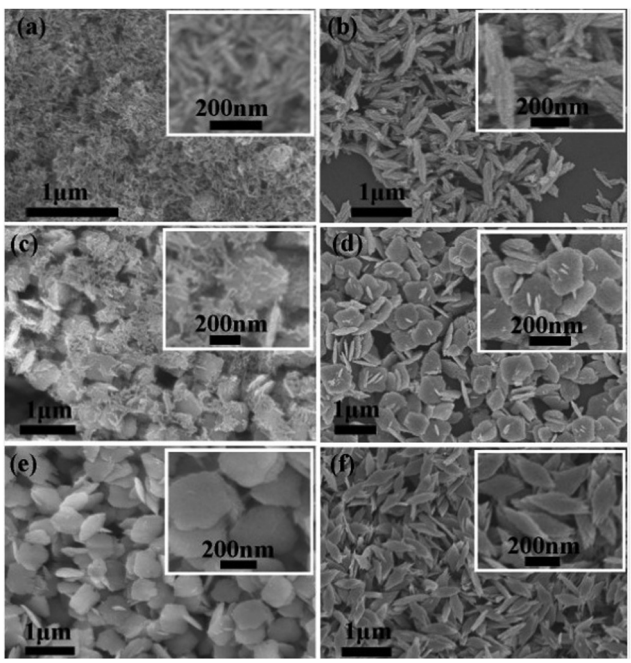


Fig. 3 FESEM images of the leaf-like copper oxide mesocrystals obtained by collagen-templated biomineralization ([collagen] = 0.5 wt%, [Cu(II)] = 0.02 mol $L^{-1}$) after different incubation times: (a) 0.5 hour; (b) 1.5 hours; (c) 3 hours; (d) 6 hours; (e) 9 hours; and (f) 12 hours.

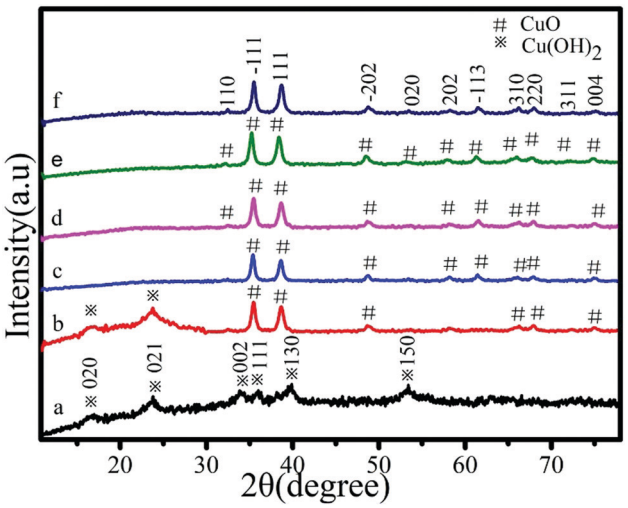


Fig. 4 XRD patterns of the leaf-like copper oxide mesocrystals obtained by collagen-templated biomineralization ([collagen] = 0.5 wt%, [Cu(II)] = 0.02 mol $L^{-1}$) after different incubation times: (a) 0.5 hours; (b) 1.5 hours; (c) 3 hours; (d) 6 hours; (e) 9 hours; and (f) 12 hours.

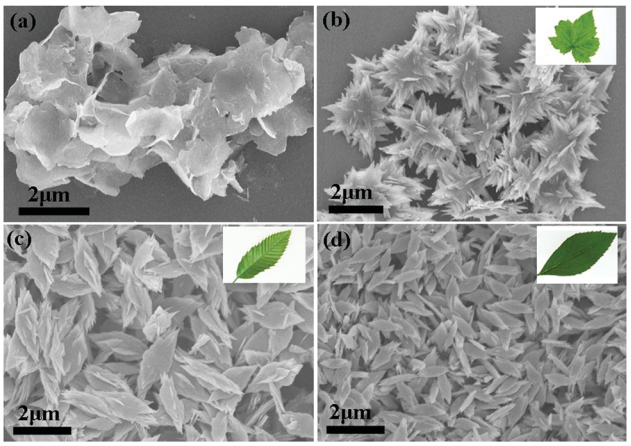


Fig. 5 FESEM images of copper oxide mesocrystals obtained after 12 hours *via* collagen-templated biomineralization with a constant Cu(II) concentration (0.02 mol $L^{-1}$) and varying concentrations of collagen: (a) 0, (b) 0.05, (c) 0.2, and (d) 0.5 wt%.

and leaf-like particles became the dominant product, whose XRD patterns corresponded to pure CuO (Fig. 3e and 4e). When the reaction was prolonged to 12 hours or longer, the CuO mesocrystals formed relatively uniform camphor leaf-like shapes (Fig. 3f and 4f).

The FESEM and XRD results of the particles synthesized *via* collagen-templated biomineralization indicated the morphological change from nanoneedles to leaf-like mesocrystals and the phase transformation from $Cu(OH)_2$ to CuO. This phase transformation probably resulted from the dehydration of $Cu(OH)_2$ under hydrothermal conditions, which has been reported in previous studies.[41] The mixture of collagen and copper acetate consistently led to the production of CuO mesocrystals with a leaf-like shape after incubation for 9 hours or longer. These results indicated that collagen may share a similar biomineralization mechanism to silk fibroin, whereas $Cu(OH)_2$ played a key precursor role for nucleation and growth of the mesocrystals.[34]

### The critical role of collagen in biomineralized CuO nanostructures

The morphologies of the CuO mesocrystals obtained using various concentrations of collagen were compared in order to evaluate the critical role of collagen in the biomineralization (Fig. 5). In the absence of collagen, only disordered CuO particles were observed (Fig. 5a). When the concentration of collagen was increased to 0.05 wt%, the CuO particles formed uniform five-star leaf-like structures (Fig. 5b). When the collagen concentration was increased to 0.2 and 0.5 wt%, the CuO particles became *Ficus* leaf-like and *Eucalyptus* leaf-like, respectively (Fig. 5c and d). The pronounced dependence of the morphology of the copper oxide mesocrystals on the concentration of collagen demonstrated that recombinant collagen could handily tune the CuO nanostructures. Collagen has been reported as the critical biotemplate for the synthesis of hydroxyapatite with hierarchical nanostructures.[38] Previous studies have shown that silk fibroin provided a nice template to modulate the shape of CuO nanoparticles.[34] These results indicated that collagen probably shared a similar mechanism, and played a key templating role in the production of CuO mesocrystals.

Thermogravimetric analysis (TGA) was carried out to measure the weight loss of CuO samples synthesized using different collagen concentrations in order to evaluate the collagen participation in the formation of the CuO nanostructures (Fig. 6). In the absence of collagen, CuO particles displayed a constant weight loss of approximately 2.2 wt%. When the collagen concentration was increased, the weight loss of CuO samples became larger accordingly. The mass loss reached about 4.8 wt% when the collagen concentration was 0.5 wt% (Fig. 6). These results indicated that collagen plays a critical

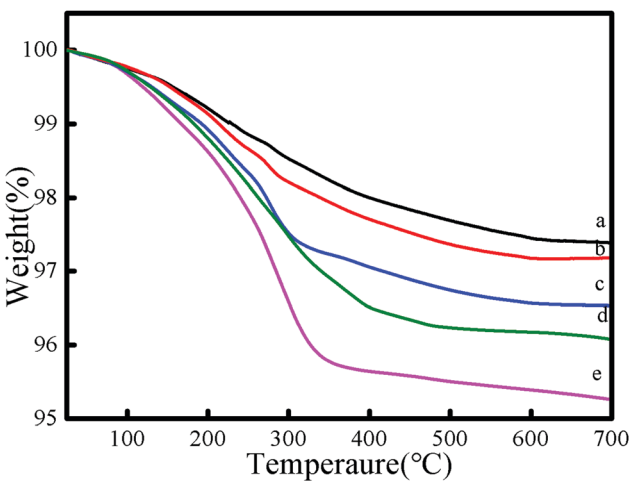


Fig. 6 TGA curves of CuO samples synthesized under various concentrations of collagen: (a) 0, (b) 0.05, (c) 0.1, (d) 0.2, and (e) 0.5 wt%.

role in the formation process of CuO nanostructures, and that a significant amount of collagen was packed within the copper oxide mesocrystals.

### The effect of copper ions on CuO nanostructures

The role of copper ions in modulating the collagen-templated synthesis of CuO mesocrystals for a constant concentration of collagen (0.1 wt%) was also examined (Fig. S4, ESI†). When the concentration of copper ions was varied in the range of 0.01–0.03 mol $L^{-1}$, the CuO mesocrystals displayed a eucalyptus leaf-like shape. When the concentration of copper ions was increased to 0.1 mol $L^{-1}$, the CuO mesocrystals became jujube-core-like. This suggested that the morphology of the CuO mesocrystals could be delicately tuned *via* the copper ion concentration in the biomineralization process.

### Electrochemical properties of CuO nanostructures

The electrochemical performance of the prepared eucalyptus leaf-like copper oxide mesocrystals was evaluated using the galvanostatic method. The galvanostatic discharge–charge cycle curves of the CuO electrode for the first 80 times were measured at 0.2C (1C = 890 mA $g^{-1}$) (Fig. 7a). The first discharge curve displayed three potential regions. The first region was 2.0–1.8 V, which indicated that $Li^+$ reacted with CuO to produce $Cu^{II}_{1-x}Cu^{I}_{x}O_{1-x/2}$ ($0 < x < 0.4$). The second (1.2–0.9 V) and third (0.9–0.001 V) regions corresponded to the formation of $Cu_2O$ and the conversion of $Cu_2O$ to Cu and $Li_2O$, respectively.[22,42,43]

The cycling performance of the CuO electrode was examined for 85 cycles at the 0.2C rate (Fig. 7b). The discharge capacity dropped at the first cycle, and gradually decreased to reach a constant value after 25 cycles. After 85 cycles, the CuO electrode maintained a high discharge capacity of 910 mAh $g^{-1}$, indicating a high capacity retention of 76%. This is one of the highest capacity retention values among all the reported anode materials that consist of pure CuO nanostructures (Table S1, ESI†). The specific capacity of the CuO electrode at different current densities was summarized (Fig. 7c). It showed a discharge capacity of 903 mAh $g^{-1}$ at a 0.1C rate after 5 cycles. When the current density was increased, the discharge capacity decreased. After 5 cycles of high current density at 2C, there was still a discharge capacity of about 300 mAh $g^{-1}$. The phenomenon probably resulted from the poor conductivity of collagen, and its effects became enhanced as the current density was increased.

As an anode material for lithium-ion batteries, the leaf-like CuO nanomaterials showed the highest initial discharge capacity (1369 mAh $g^{-1}$) as well as reversible capacity (1041 mAh $g^{-1}$) at a 0.2C rate when compared with other previously reported CuO nanostructures. In addition, the CuO nanomaterials showed good cycling stability, and maintained a discharge capacity as high as 910 mAh $g^{-1}$, even after 85 cycles. This was among the highest final discharge capacity values for all the reported CuO nanostructures (Table S1, ESI†).

The as-prepared leaf-like CuO mesocrystals exhibited excellent electrochemical features, which may result from their unique morphology. First, the CuO mesocrystals provided

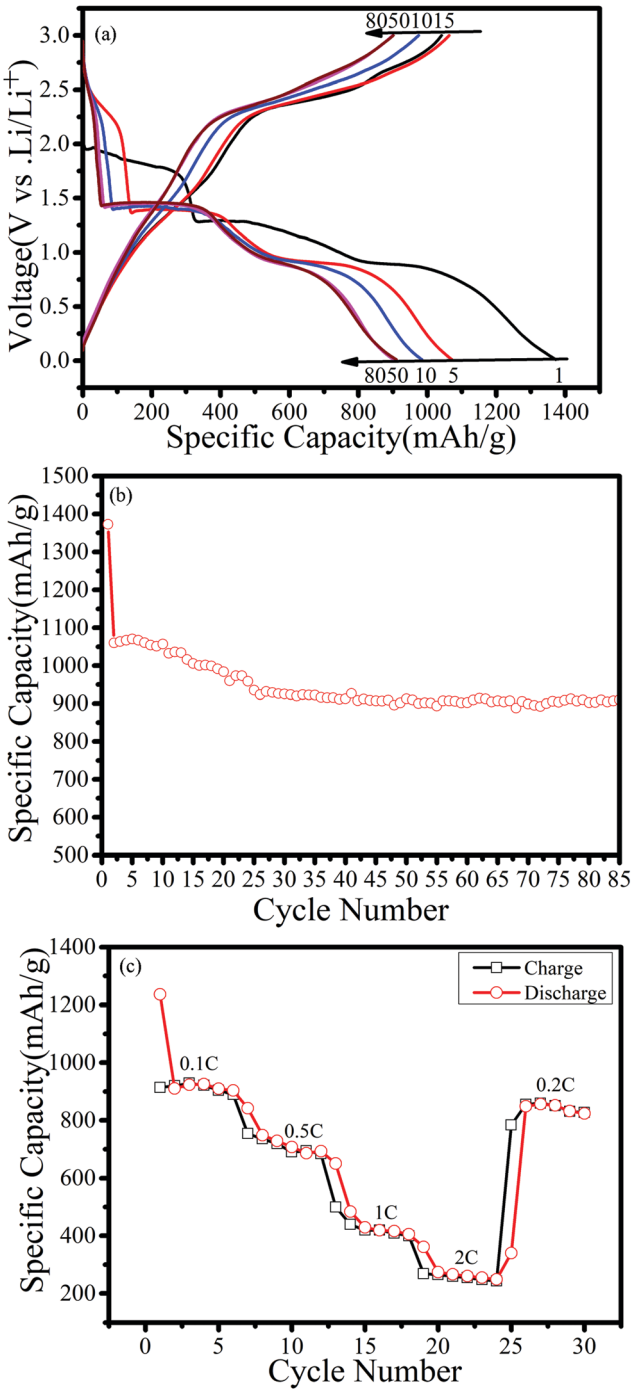


Fig. 7 Electrochemical properties of the CuO electrode. (a) Voltage profiles of the CuO electrode for different charge–discharge cycles at the current rate at 0.2C; (b) specific discharge capacity of the CuO electrode for the first 85 cycles at 0.2C; and (c) specific capacity as a function of cycle number and charging (black open squares) or discharging (red open circles) at various rates. The rate for the first discharge process was set at 0.1C, and then the rate was respectively increased to 0.5, 1, and 2C in the voltage range of 0.001–3 V.

better accommodation of the strain energy and proper electrode–electrolyte contact area, and decreased the polarization of the electrode during the charge–discharge cycles. Second,

the CuO mesocrystals consisted of orderly packed 2D nanoplates, leading to a shorter lithium-ion diffusion path and faster surface electrochemical reactions, therefore enhancing the capacity during the charge–discharge process. Meanwhile, the leaf-like CuO mesocrystals may resist particle pulverization and agglomeration during cycling.[44,45] Previous studies have suggested that the extra capacity could result from the reversible transformation of polymeric gel-like films.[46] Further studies also revealed that transition metal nanoparticles may act as efficient electrocatalysts to activate and/or promote the reversible transformation of some inorganic components in SEI films.[47–49] These factors could contribute to the increasing capacity for lithium storage.

### Biocompatibility and bioactivity of the leaf-like CuO

The biocompatibility and bioactivity of the as-prepared leaf-like CuO nanomaterials was further investigated (Fig. 8). The *in vitro* cytotoxicity of leaf-like CuO nanomaterials was evaluated by examining the viability of HFF-1 cells using the CCK-8 assays (Fig. 8a). The leaf-like CuO showed a similarly high cell viability at four different concentrations (0.1, 1, 10, and 100 μg $mL^{-1}$), indicating that the as-prepared leaf-like CuO nanomaterials have good biocompatibility (Fig. 8a). This suggested that the inclusion of the natural protein collagen in the CuO nanomaterials probably provided the high biocompatibility.

Collagen is a key structural and functional protein in the human body. The bioactivity of leaf-like CuO nanomaterials was determined *via* a cell-adhesion assay using HFF-1 cells (Fig. 8b). HFF-1 cells were cultured on the plate wells coated with leaf-like CuO and heat-denatured bovine serum albumin (BSA). The fluorescence intensity of the wells coated with leaf-like CuO was much higher than those coated with the control BSA, demonstrating that HFF-1 cells could efficiently attach to the as-prepared leaf-like CuO nanomaterials (Fig. 8b). This indicated that collagen can effectively functionalize CuO nanomaterials with cell-adhesion bioactivity.

Cell adhesion and spreading features were examined using confocal fluorescence microscopy (Fig. 8c and d). HFF-1 cells were fixed and stained for actin stress fibers and nuclei using phalloidin-tetramethylrhodamine isothiocyanate and DAPI, respectively. The HFF-1 cells on the CuO-coated substrates showed a well-developed actin cytoskeletal structure (Fig. 8c and d). The extensive cell adhesion and spreading demonstrated that collagen endowed the CuO nanomaterials with a superior biofunction. These results indicated that collagen not only provides a robust template to modulate the nanostructures of CuO but also acts as a functional agent to endow the prepared nanomaterials with attractive bioactivity.

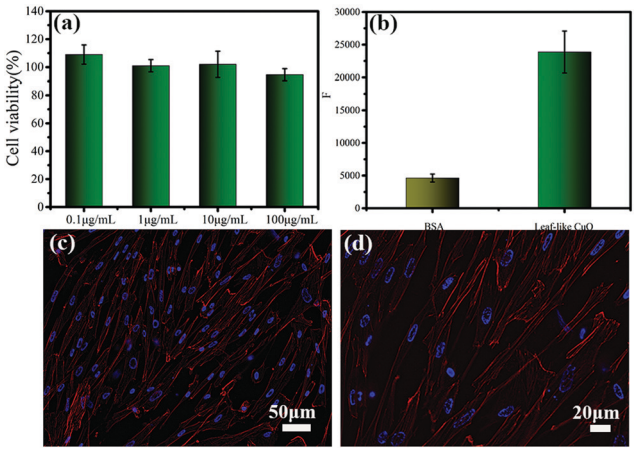


Fig. 8 Biocompatibility and bioactivity of the leaf-like CuO. The *in vitro* cytotoxicity of leaf-like CuO nanomaterials with different concentrations was evaluated by examining the viability of HFF-1 cells (a). The adhesion ability of HFF-1 cells to leaf-like CuO nanomaterials *versus* the control BSA (b). Adhesion and spreading of HFF-1 cells on the surface of leaf-like CuO materials (c and d). Cells were fixed and stained for actin stress fibers (red) and nuclei (blue).

## 4. Conclusion

In conclusion, copper oxide mesocrystals with novel hierarchical structures have been successfully created using a biomineralization approach with recombinant collagen as the template. We have demonstrated that the nanostructures of copper oxide particles can be finely modulated *via* the collagen concentration (Scheme 1). Collagen-templated biomineralization probably displays a similar mechanism to that reported for silk fibroin.[34] First, Cu(II) ions form a complex with collagen by interaction with polar amino acids when copper acetate is added to the collagen solution. Then, the addition of sodium hydroxide drives $Cu^{2+}$ to form $Cu(OH)_2$, which possesses a nanoneedle-like structure due to the interaction of $Cu^{2+}$ and the collagen biotemplate. Third, the $Cu(OH)_2$ is further assembled into a primary nanostructure, which is dehydrated into CuO in the meantime. Finally, the free CuO in the reaction solution gets crystallized on the primary nanostructure, leading to the formation of larger leaf-like mesocrystals. The primary nanostructure is formed using collagen as the template, therefore leading to a more ordered, compact middle region. By contrast, the later crystallization of free CuO lacks the assistance of the collagen template, and results in loose ends. During the collagen-templated biomineralization process of

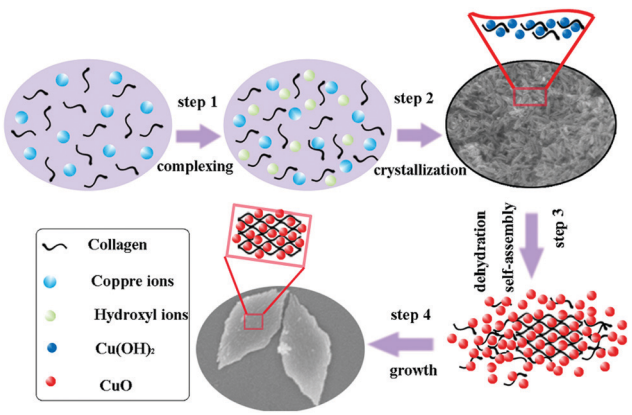


Scheme 1 Illustration of the critical role of collagen in the mediation of hierarchical nanostructures of copper oxide mesocrystals.

CuO nanoparticles, formation of the complex between Cu(II) and collagen seems to play a determining role.

Collagen provides a superior biotemplate for the production of copper oxide nanocrystals. Compared with silk fibroin, collagen is able to regulate the hierarchical structures of copper oxide mesocrystals with a much lower concentration, and collagen can produce a much richer diversity of hierarchical nanostructures.[34] Compared with previously reported proteins, collagen contains a large number of charged amino acids, which may promote the interaction of copper ions and collagen. Furthermore, the distinct $(Gly\text{-}X\text{-}Y)_n$ amino acid sequence pattern and the triple-helix structure may provide a unique capability for collagen in protein-templated biomineralization. In addition, recombinant technology can produce collagen of a single size and high purity, and it can be used to easily modify the amino acid sequences of collagen.[40,50] Therefore, recombinant collagen may provide a powerful strategy for creating superior biotemplates.

Notably, the novel leaf-like CuO mesocrystals prepared *via* collagen-assisted biomineralization show excellent biofunctional and electrochemical properties. Advanced health-care devices such as cardiac peacemakers, neuro-stimulators and hearing aids have been received increasing attention, while the development of high-performance biocompatible batteries is of pivotal importance. We have for the first time discovered that the unique protein collagen not only provides an excellent template to create CuO nanomaterials with exquisite morphology, but also functionalizes them with high biocompatibility and bioactivity. The newly developed environmentally friendly method assisted by collagen provides excellent opportunities for the construction of advanced high-performance biofunctional CuO nanomaterials, which may have great potential in implantable health-care electronic systems.

## Conflicts of interest

The authors declare no competing conflict of interests.

## Acknowledgements

This work was supported by grants from the National Natural Science Foundation of China (Grant No. 22074057, and 21775059), the National Natural Science Foundation of Gansu Province (Grant No. 20YF3FA025, and 18YF1NA004), and the Lanzhou Talent Innovation and Entrepreneurship Project (Grant No. 2019-RC-43).

## References

1 D. Gebauer and H. Colfen, *Nano Today*, 2011, **6**, 564–584.
2 Y. Oaki, A. Kotachi, T. Miura and H. Imai, *Adv. Funct. Mater.*, 2006, **16**, 1633–1639.
3 M. B. Dickerson, K. H. Sandhage and R. R. Naik, *Chem. Rev.*, 2008, **108**, 4935–4978.
4 C. Y. Chiu, Y. J. Li, L. Y. Ruan, X. C. Ye, C. B. Murray and Y. Huang, *Nat. Chem.*, 2011, **3**, 393–399.
5 J. Ge, J. D. Lei and R. N. Zare, *Nat. Nanotechnol.*, 2012, **7**, 428–432.
6 M. M. Tomczak, J. M. Slocik, M. D. Stone and R. R. Naik, *Biochem. Soc. Trans.*, 2007, **35**, 512–515.
7 C. Achtel, S. M. Harling, W. Hering, M. Westerhausen and T. Heinze, *Macromol. Rapid Commun.*, 2018, **39**, 1605544.
8 S. Lagziel-Simis, N. Cohen-Hadar, H. Moscovich-Dagan, Y. Wine and A. Freeman, *Curr. Opin. Biotechnol.*, 2006, **17**, 569–573.
9 L. A. Estroff and A. D. Hamilton, *Chem. Mater.*, 2001, **13**, 3227–3235.
10 M. Auffan, J. Rose, J. Y. Bottero, G. V. Lowry, J. P. Jolivet and M. R. Wiesner, *Nat. Nanotechnol.*, 2009, **4**, 634–641.
11 Y. Gong, M. F. Zhou and L. Andrews, *Chem. Rev.*, 2009, **109**, 6765–6808.
12 A. Loiudice, S. Saris and R. Buonsanti, *J. Phys. Chem. Lett.*, 2020, **11**, 3430–3435.
13 Y. Zhong, Y. F. Ma, Q. B. Guo, J. Q. Liu, Y. D. Wang, M. Yang and H. Xia, *Sci. Rep.*, 2017, **7**, 40927.
14 Y. Jiang, J. L. Yue, Q. B. Guo, Q. Y. Xia, C. Zhou, T. Feng, J. Xu and H. Xia, *Small*, 2018, **14**, 1704296.
15 H. Yi, Y. Huang, Z. C. Sha, X. H. Zhu, Q. Y. Xia and H. Xia, *Mater. Lett.*, 2020, **276**, 128205.
16 F. Zan, N. Jabeen, W. Xiong, A. Hussain, Y. D. Wang and H. Xia, *Nanotechnology*, 2020, **31**, 185402.
17 S. Venkatachalam, H. W. Zhu, C. Masarapu, K. H. Hung, Z. Liu, K. Suenaga and B. Q. Wei, *ACS Nano*, 2009, **3**, 2177–2184.
18 S. Sahoo, S. Husale, B. Colwill, T. M. Lu, S. Nayak and P. M. Ajayan, *ACS Nano*, 2009, **3**, 3935–3944.
19 D. D. Li, J. Hu, R. Q. Wu and J. G. Lu, *Nanotechnology*, 2010, **21**, 485502.
20 M. J. Song, S. W. Hwang and D. Whang, *Talanta*, 2010, **80**, 1648–1652.
21 W. X. Zhang, M. Li, Q. Wang, G. D. Chen, M. Kong, Z. H. Yang and S. Mann, *Adv. Funct. Mater.*, 2011, **21**, 3516–3523.
22 L. L. Wang, W. Cheng, H. X. Gong, C. H. Wang, D. Wang, K. B. Tang and Y. T. Qian, *J. Mater. Chem.*, 2012, **22**, 11297–11302.
23 R. V. Kumar, R. Elgamiel, Y. Diamant, A. Gedanken and J. Norwig, *Langmuir*, 2001, **17**, 1406–1410.
24 W. X. Zhang, X. G. Wen, S. H. Yang, Y. Berta and Z. L. Wang, *Adv. Mater.*, 2003, **15**, 822–825.
25 B. Liu and H. C. Zeng, *J. Am. Chem. Soc.*, 2004, **126**, 8124–8125.
26 L. P. Xu, S. Sithambaram, Y. S. Zhang, C. H. Chen, L. Jin, R. Joesten and S. L. Suib, *Chem. Mater.*, 2009, **21**, 1253–1259.
27 J. Y. Li, S. L. Xiong, B. J. Xi, X. G. Li and Y. T. Qian, *Cryst. Growth Des.*, 2009, **9**, 4108–4115.
28 D. P. Singh, A. K. Ojha and O. N. Srivastava, *J. Phys. Chem. C*, 2009, **113**, 3409–3418.
29 G. R. Bourret and R. B. Lennox, *J. Am. Chem. Soc.*, 2010, **132**, 6657–6666.
30 Z. Y. Wang, F. B. Su, S. Madhavi and X. W. Lou, *Nanoscale*, 2011, **3**, 1618–1623.

31 X. Chen, N. Q. Zhang and K. N. Sun, *J. Mater. Chem.*, 2012, **22**, 13637–13642.
32 M. Vaseem, A. Umar, S. H. Kim and Y. B. Hahn, *J. Phys. Chem. C*, 2008, **112**, 5729–5735.
33 H. H. Wang, Q. Shen, X. P. Li and F. L. Liu, *Langmuir*, 2009, **25**, 3152–3158.
34 X. Fei, Z. Z. Shao and X. Chen, *Nanoscale*, 2013, **5**, 7991–7997.
35 B. Brodsky and J. A. M. Ramshaw, *Matrix Biol.*, 1997, **15**, 545–554.
36 M. D. Shoulders and R. T. Raines, *Annu. Rev. Biochem.*, 2009, **78**, 929–958.
37 E. A. Zimmermann and R. O. Ritchie, *Adv. Healthcare Mater.*, 2015, **4**, 1287–1304.
38 M. M. He, Y. P. Zhang, J. C. Munyemana, T. Wu, Z. F. Yang, H. J. Chen, W. P. Qu and J. X. Xiao, *J. Mater. Chem. B*, 2017, **5**, 1423–1429.
39 A. Yoshizumi, Z. X. Yu, T. Silva, G. Thiagarajan, J. A. M. Ramshaw, M. Inouye and B. Brodsky, *Protein Sci.*, 2009, **18**, 1241–1251.
40 Y. Y. Peng, L. Howell, V. Stoichevska, J. A. Werkmeister, G. J. Dumsday and J. A. M. Ramshaw, *Microb. Cell Fact.*, 2012, **11**, 146.
41 C. H. Lu, L. M. Qi, J. H. Yang, D. Y. Zhang, N. Z. Wu and J. M. Ma, *J. Phys. Chem. B*, 2004, **108**, 17825–17831.
42 F. S. Ke, L. Huang, G. Z. Wei, L. J. Xue, J. T. Li, B. Zhang, S. R. Chen, X. Y. Fan and S. G. Sun, *Electrochim. Acta*, 2009, **54**, 5825–5829.
43 E. Garcia-Tamayo, M. Valvo, U. Lafont, C. Locati, D. Munao and E. M. Kelder, *J. Power Sources*, 2011, **196**, 6425–6432.
44 H. Ma, S. Y. Zhang, W. Q. Ji, Z. L. Tao and J. Chen, *J. Am. Chem. Soc.*, 2008, **130**, 5361–5367.
45 J. Jamnik, R. Dominko, B. Erjavec, M. Remskar, A. Pintar and M. Gaberscek, *Adv. Mater.*, 2009, **21**, 2715–2719.
46 S. Laruelle, S. Grugeon, P. Poizot, M. Dolle, L. Dupont and J. M. Tarascon, *J. Electrochem. Soc.*, 2002, **149**, A627–A634.
47 L. W. Su, Z. Zhou, X. Qin, Q. W. Tang, D. H. Wu and P. W. Shen, *Nano Energy*, 2013, **2**, 276–282.
48 L. W. Su, Y. R. Zhong and Z. Zhou, *J. Mater. Chem. A*, 2013, **1**, 15158–15166.
49 L. W. Su, J. P. Hei, X. B. Wu, L. B. Wang and Z. Zhou, *Adv. Funct. Mater.*, 2017, **27**, 1065544.
50 J. A. M. Ramshaw, Y. Y. Peng, V. Glattauer and J. A. Werkmeister, *J. Mater. Sci.: Mater. Med.*, 2009, **20**, 3–8.